International Journal of Biological Macromolecules 117 (2018) 1017–1028

Contents lists available at ScienceDirect

International Journal of Biological Macromolecules

journal homepage: http://www.elsevier.com/locate/ijbiomac

Evaluation of chitosan and carboxymethyl cellulose as ecofriendly corrosion inhibitors for steel

Saviour A. Umoren [a,*], Abdullah A. AlAhmary [b], Zuhair M. Gasem [b], Moses M. Solomon [a]

[a] Center of Research Excellence in Corrosion, Research Institute, King Fahd University of Petroleum and Minerals, Dhahran 31261, Saudi Arabia
[b] Department of Mechanical Engineering, Faculty of Engineering, King Fahd University of Petroleum and Minerals, Dhahran 31261, Saudi Arabia

ARTICLE INFO

Article history:
Received 15 March 2018
Received in revised form 28 May 2018
Accepted 4 June 2018
Available online 5 June 2018

Keywords:
Polymers
Corrosion inhibitors
Chitosan
Carboxymethyl cellulose
Sweet corrosion
Carbon steel

ABSTRACT

The study was aimed at establishing the possibility of using eco-friendly natural polymers to formulate corrosion inhibitors for sweet oil field environment. Against this background, the performance of two natural polymers; chitosan and carboxymethyl cellulose (CMC) as single component corrosion inhibitors in comparison with a commercial inhibitor formulations, on API 5L X60 pipeline steel in CO_2 saturated 3.5% NaCl solution were investigated using electrochemical impedance spectroscopy (EIS) and potentiodynamic polarization (PDP) techniques; complemented with surface morphology characterization of the corroded steel samples without and with inhibitors using scanning electron microscope (SEM). The results indicate that there is a remarkable difference in inhibition efficiency of each inhibitor on the API 5L X60 steel and the commercial inhibitor formulations. Inhibition efficiency increased with the increase of inhibitors' concentrations. Immersion time was found to have a profound effect on the corrosion inhibition performance of all the inhibitors. Also the inhibition efficiency was found to decrease with the increase in temperature. Potentiodynamic polarization results reveal a mixed-type inhibition for all inhibitors. The adsorption of each inhibitor on the steel surface obeys Langmuir's isotherm.

1. Introduction

Carbon steel is widely used in the oil and gas industry for different purposes. Its huge usage can be attributed to its endearing properties which include hardness, durability, ductility, low cost and handiness. However, they are highly susceptible to corrosion in the service environment to which they are deployed thereby limiting their end-use. The most frequent aggressive environments found in the petroleum industry are those of fluids with high concentrations of chlorides containing carbon dioxide (CO_2) [1]. CO_2 gas dissolves in the associated salt water and forms a weak carbonic acid which leads to severe corrosion attack which may be general or localized in nature.

One of the cost-effective methods for controlling carbon steel corrosion caused by CO_2 in the oil and gas production is the use of chemical corrosion inhibitors [2]. Literature reports have shown that nitrogen based organic inhibitors, such as amines and imidazolines or their salts, have been the most profitably used to inhibit CO_2 corrosion occurring in internal pipelines [3–14]. Although these inhibitors are stable and provide adequate protection in corrosive environments [15, 16], they can be very costly to formulate and are not environmentally friendly due to their toxic nature. Most of them do persist in the environment and require expensive processes for their removal [17]. Due to problems associated with commercial corrosion inhibitors, research interest is now geared towards developing environmentally friendly corrosion inhibitors from natural sources by reformulating the existing products or by identifying new chemistries for developing safer products [18]. Natural polymers could serve as good alternative for toxic organic corrosion inhibitors. Natural polymers are compatible with the natural ecosystem; occur in large amount and their prices are affordable. Also, they possess multiple adsorption sites which should make them easily adsorbable. The use of natural polymers as corrosion inhibitors for carbon steel in acid media could be found in the literature [19–24]. We have also documented a comprehensive review on the use of biopolymers as corrosion inhibitors for metals in different corrosive media [28]. However, the use of natural polymers to mitigate sweet (CO_2) corrosion for steel in saline media is scanty [25].

The present work was undertaken to evaluate the corrosion protective abilities of two single component and green inhibitor compounds, chitosan and carboxymethyl cellulose (CMC) compared with a multiple-component and commercially available corrosion inhibitor (NALCO Product, US) with the intent that if these simple and green single-component compounds could show remarkably high corrosion protection in CO_2 saturated saline solution for API 5L X60 pipeline steel compared to commercial inhibitor, they could serve as active components in corrosion inhibitor formulations for practical industrial applications.

* Corresponding author.
E-mail address: umoren@kfupm.edu.sa (S.A. Umoren).

https://doi.org/10.1016/j.ijbiomac.2018.06.014
0141-8130/

2. Experimental

2.1. Materials and materials preparation

Two natural polymers namely chitosan and carboxyl methylcellulose (CMC) with chemical structure of their repeat unit shown in Fig. 1 and commercial inhibitor formulation were employed as test inhibitors. Chitosan with ≥75.0% as the degree of deacetylation and CMC were obtained from Sigma-Aldrich and they have molecular weight of 50,000–190,000 Da (based on viscosity) and ~90,000 g/mol respectively. The commercial inhibitor was supplied by NALCO holding company, USA. The metal substrate was low carbon (API 5L X60 grade) steel substrate typically used as oil pipeline material with chemical composition as earlier reported [26]. A deoxygenated and CO_2 saturated 3.5 wt% NaCl solution was employed as the corrosive medium.

2.2. Electrochemical tests

All electrochemical measurements were performed using Gamry potentiostat/galvanostat/ZRA (Reference 3000) in a glass cell with a three electrode set-up, with platinum and saturated calomel electrode used as the counter and reference electrodes respectively. In order to simulate the de-aerated oilfield environment, the solution was first purged with N_2 (99.99%) for 30 min. This ensured low concentration of dissolved oxygen to mimic the produced oilfield fluid [27]. This was followed by purging with CO_2 gas to saturate the environment for 2 h before the insertion of the working electrode into the test solution. The pH was about 3.8 when the solution was saturated with CO_2 and was adjusted to the working pH of 5.0 by addition of sodium bicarbonate ($NaHCO_3$). The CO_2 gas was bubbled continuously throughout the experiment. Prior to each measurement, a stable Open Circuit Potential (OCP) was reached within 1 h after the sample was immersed in the test solution. Electrochemical Impedance Spectroscopy (EIS) experiments were performed under potentiostatic condition between 100000 Hz to 0.1 Hz with a small amplitude perturbation 10 mV (peak-to-peak) for an AC signal at E_{corr}. Potentiodynamic polarization measurement was carried out from cathodic potential of −250 mV to anodic potential of +250 mV with respect to the corrosion potential at a sweep rate of 1 mV/s.

Inhibition efficiency (*IE*%) from the electrochemical measurements was computed using Eqs. (1) and (2) for electrochemical impedance spectroscopy and potentiodynamic polarization measurements respectively:

$$IE = \left(1 - \frac{R_p^0}{R_p}\right) \times 100 \quad (1)$$

$$IE = \left(1 - \frac{i_{corr}}{i_{corr}^0}\right) \times 100 \quad (2)$$

where R^0_p and i^0_{corr} are the polarization resistance and corrosion current density in the absence of additives, R_p and i_{corr}, the polarization resistance and corrosion current density in the presence of additives respectively [28, 29].

2.3. Surface characterization

The API 5L X60 steel specimen abraded up to 1000 grit size SiC paper were immersed for 24 h at 25 °C in 3.5% NaCl saturated with CO_2 with and without the test inhibitors. After 24 h immersion time, the samples were removed from the solution, rinsed with distilled water and dried at room temperature and submitted for the surface analysis using Scanning Electron Microscopy (JOEL JSM-6610LV) operated at accelerating voltage of 20 kV.

3. Results and discussion

3.1. Effect of inhibitor concentration

The effect of increment in the amount of each inhibitor against the corrosion of API 5L X60 steel in 3.5% NaCl solution saturated with CO_2 was investigated using EIS technique at 25 °C. Fig. 2 present the impedance plots for API 5L X60 steel in CO_2-saturated 3.5% NaCl solution in the absence and presence of varying concentrations of chitosan, CMC and commercial inhibitor in (a–c) Nyquist, (d–f) Bode and (g–i) phase angle representations. The shape of the Nyquist plots for the three tested inhibitors are similar indicative of an unchanged mechanism of protection as their concentrations increased. Larger diameters of Nyquist semi-circles are attributes of higher corrosion resistance systems of inhibitors compared to the blank solution, and in this study, higher concentrations of these inhibitors possess wider Nyquist curve widths showing dependence of concentration on the corrosion process. This electrochemical change is indicative of inhibition of corrosion process at increased concentration of the inhibitors by adsorbing on the surface of the metal thereby reducing the active surface area exposed to the aggressive corrosive electrolyte medium [28]. The reason for the relative distortions of the semi-circles could be attributed to the unevenness of the metal surface, and this phenomenon has been elaborately explained elsewhere [30]. Moreover, higher impedance values for the Nyquist curves obtained were recorded for the commercial corrosion inhibitor (Fig. 2(c)) to two folds of a thousand compared to chitosan and CMC. The reason for this varying superior resistance and protective performance in the presence of corrosive chloride ions and CO_2 could be due to the fact that Chitosan and CMC are single component substances which are relatively small water-soluble and linear polysaccharide compounds bearing simple amino and carboxymethyl groups, respectively, for less stronger metal surface interactions, while commercial inhibitor is an oil-based hybrid composite formulations consisting of active inhibitors, surfactant, enhancers, wetting agents and modifiers in methanol. The commercial inhibitor is a highly viscous suspension widely used in

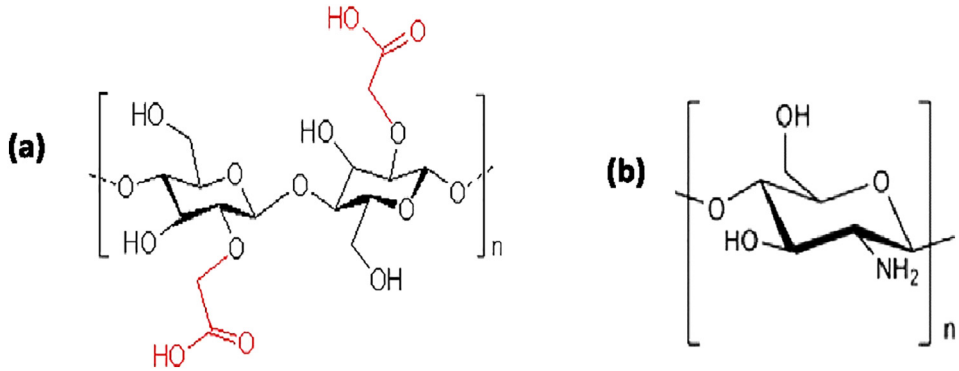

Fig. 1. Chemical structure of (a) CMC and (b) Chitosan repeat unit.

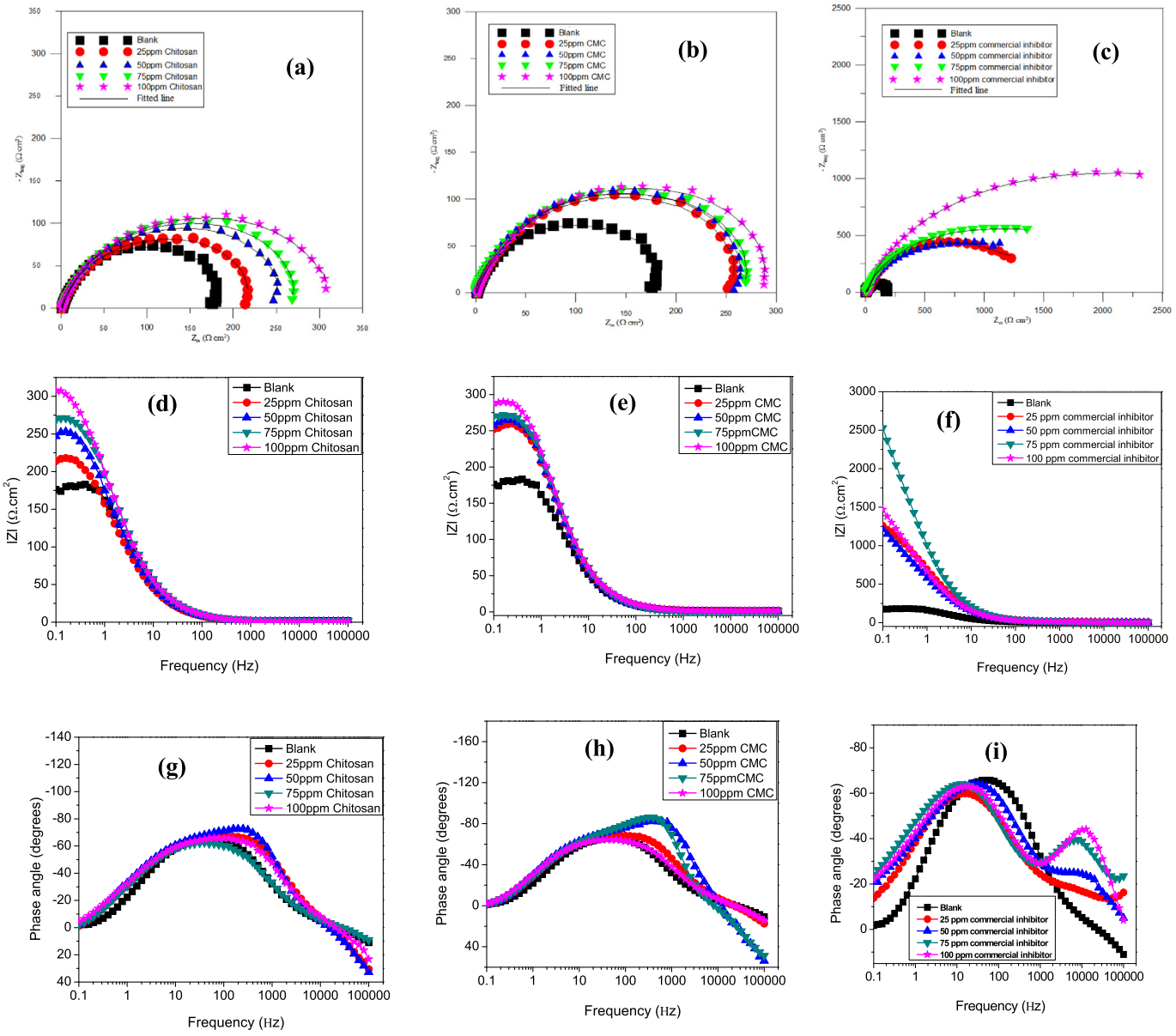

Fig. 2. Impedance plots for API 5L X60 steel in CO_2-saturated 3.5% NaCl solution in the absence and presence of varying concentrations of Chitosan, CMC and commercial inhibitor in (a) Nyquist, (b) Bode and (c) phase angle representations at 25 °C.

many complex oil-field based corrosion control and thus, remains a baseline protective pigment for the design and development of other field and lab-based inhibitor formulation. Chitosan and CMC were chosen to study comparatively with commercial inhibitor because of their unique electronic and molecular structures since their anticorrosive properties as compounds are largely linked with their chemical makeup (Fig. 1). Distinctly, the β-(1-4)-linked D-glucosamine/*N*-acetyl-D-glucosamine and carboxymethyl-bound glucopyranyl moieties on chitosan and CMC, respectively, bear some O and N heteroatoms capable of adsorption at the surface of API 5L X60 steel thereby forming a mass/charge barrier against further corrosive attack, hence inhibition. Apart from being multifunctional group compounds, Chitosan and CMC are green, stable, benign and biodegradable inhibitors.

Equivalent circuit models provide an insight into the significance of the variation of impedance parameters from each response derived from the EIS spectra. The circuit model employed in fitting experimental data for the inhibiting system (Fig. 3b) consists of R_f and CPE_f in parallel representing the adsorbed species forming films on the surface of API 5L X60 steel in the solution of the electrolyte with resistance (R_s); the charge transfer resistance (R_{ct}) and its double layer constant phase element component (CPE_{dl}) in parallel to the first set of components. For the equivalent circuit of this nature, the polarization resistance (R_p) is given as [31]:

$$R_p = R_f + R_{ct} \tag{3}$$

The simple Randel circuit (Fig. 3a) was employed in fitting the impedance data without the inhibitors (blank solutions). The CPE is used in place of a capacitor to account for the deviations from ideal dielectric behavior due to heterogeneous nature of the working electrode surface. The impedance of the *CPE* is given as follows [32]:

$$Z_{CPE} = Y_o^{-1}(j\omega)^{-n} \tag{4}$$

where Y_0 is the CPE constant and n the CPE exponent; $j = (-1)^{½}$ which is an imaginary number and ω is the angular frequency in rad/s ($\omega = 2\pi f$), where f is the frequency in Hz. The CPE can be a resistance, capacitance, Warburg impedance or inductance if n is equaled to 0, 1, 0.5 or −1 respectively.

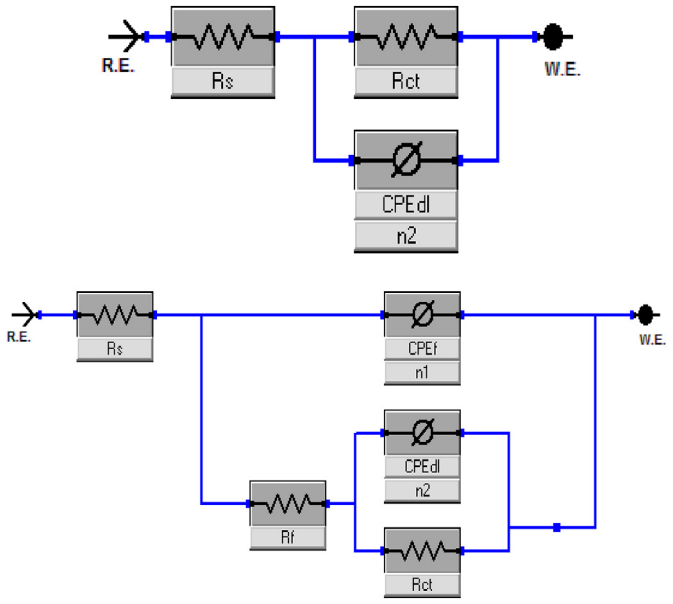

Fig. 3. Equivalent circuit models used in fitting EIS experimental data for (a) blank and (b) inhibiting systems.

The derived electrochemical parameters from Nyquist plots are listed in Table 1. From the enlisted electrochemical data, the increase in the values of R_p at the electrode/electrolyte interface is found to increase with the concentration of each inhibitor up to 100 ppm, except for commercial inhibitor which is 75 ppm and then drops for the highest concentration. However, decrease in R_p values for 100 ppm commercial inhibitor indicates a saturation of the adsorbed film at the electrode surface. At this concentration, the adsorbed species must have saturated the electrode surface and thus, become porous due to constant corrosive attack in the presence of the CO_2 gas. Again, the increase in the values of R_p with concentration of the inhibitors confirms corrosion inhibition. Values of R_p for the three tested inhibitors are in this order: Commercial inhibitor ≫ Chitosan > CMC; showing that the commercial inhibitor formulations used in oilfields protects API 5L X60 pipeline steel better from sweet corrosion. Nevertheless, the natural polymers, chitosan and CMC are promising corrosion inhibitors for API 5L X60 pipeline steel since as single component could afford R_p of 337 Ω cm^2 and 304 Ω cm^2 relative to 1610 Ω cm^2 for the commercial inhibitor. Most commercial inhibitors are multi-component formulations.

Phase angle plots are used to show the frequency-independent phase shift between the applied potential and its corresponding current response in EIS spectra; when the phase angle ≈ 90°, the current passes through a capacitor, and the metal/electrolyte interface could be considered to be capacitive [33]. We can see in the phase diagrams (Fig. 2(g–i)) that the inhibitor systems under study showed wide capacitive behavior, with phase angle close to 90° for every concentration. This behavior is related to the extent of the replacement of water molecules at the metal surface (Eq. 5) which could be done by any of these two ways or both. First, the heteroatoms (O in CMC; O and N in chitosan) could adsorb onto the sample surface by donating pi-electron (s) to Fe atoms and accepting electrons from 3d orbits of the Fe atoms [3]. Second, in the test solution, the inhibitor molecules through their heteroatoms could combine with hydrogen ions to exist in cationic form. As explained by Pojtanabuntoeng and Salasi [34], the initial step of CO_2 corrosion involves the dissolution of CO_2 into the liquid phase followed by hydration to form carbonic acid (H_2CO_3). The H_2CO_3 dissociates to give HCO_3^-, CO_2^{3-}, and H^+. The protonated inhibitor molecules could also adsorb onto negatively charged steel surface [22]. At lower frequencies for each system, phase angle gradually drops, reaching 0° for all the inhibitors, except for chitosan. At lower frequencies, the most inhibiting concentrations of each system should have the lowest phase angle compared to the blank, hence reduced corrosion phenomena at the metal/solution interface [33, 35]. The trend in phase angle has shown that the performance of chitosan and CMC is similar on the API 5L X60 pipeline steel in CO_2-saturated saline solution.

The potentiodynamic polarization curves for API 5L X60 steel in CO_2-saturated 3.5% NaCl solution in the absence and presence of varying concentrations of (a) chitosan, (b) CMC and (c) commercial inhibitor is displayed in Fig. 4. The curves show active anodic behavior, with the current density increasing as the potential is applied, without a distinctive transition to passivation within the potential range studied. The hydration of CO_2 to provide carbonic acid in the solution of the electrolyte follows Eq. (5), and the cathodic reaction is the H^+ reduction enhanced by the carbonic acid dissociation in de-aerated electrolytes (Eqs. (5)–(8)) [36].

$$CO_2 + H_2O \rightarrow H_2CO_3 \quad (5)$$

$$H_2CO_3 \rightarrow H^+ + HCO_3^- \quad (6)$$

$$HCO_3^- \rightarrow H^+ + CO_3^{2-} \quad (7)$$

$$H^+ + e^- \rightarrow {}^1/_2 H_2 \quad (8)$$

However, the cathodic curves do not exhibit well defined Tafel regions as such only the linear parts of the anodic branches were used to evaluate the potentiodynamic characteristics [37]. From the corrosion current (I_{corr}) obtained from the analysis, the corrosion current density (i_{corr}) was calculated using the following equation [37]:

$$i_{corr} = \frac{I_{corr}}{\rho} \quad (9)$$

Table 1
EIS parameters for API 5L X60 steel corrosion in CO_2-saturated 3.5% NaCl solution without and with different concentrations of chitosan, CMC and commercial inhibitor at 25 °C.

Specimen	Concentration (ppm)	R_s (Ω cm^2)	CPE_f		R_f (Ω cm^2)	CPE_{dl}		R_{ct} (Ω cm^2)	$\chi^2 \times 10^{-3}$	R_p (Ω cm^2)	IE (%)
			$Yo1$ (μΩ s^n cm^{-2})	n_f		$Yo2$ (μΩ s^n cm^{-2})	n_{dl}				
Blank	–	1.5	–	–	–	521	0.85	186.9	2.74	187	–
Chitosan	25	0.7	224	0.95	15.4	747	0.70	225.5	16.30	241	22
	50	1.9	589	0.80	50.7	864	0.99	233.3	2.34	284	34
	75	1.9	406	1.00	76.6	707	0.74	240.9	18.24	318	41
	100	1.0	103	1.00	5.2	723	0.67	331.7	8.59	337	45
CMC	25	1.0	228	0.93	40.4	363	0.79	226.8	5.44	267	28
	50	0.3	180	1.00	54.5	442	0.83	219.1	6.21	274	32
	75	0.5	190	1.00	91.6	573	0.84	186.8	6.41	278	33
	100	1.6	266	0.89	32.2	322	0.74	272.0	4.01	304	39
Commercial inhibitor	25	5.9	155	0.64	12.4	118	0.82	1404.0	1.24	1416	87
	50	2.6	355	0.62	13.1	37	0.99	1494.0	1.04	1507	87
	75	3.2	23	0.80	19.7	169	0.78	2833.0	3.20	2853	93
	100	2.0	4	1.00	9.3	281	0.76	1601.0	2.76	1610	88

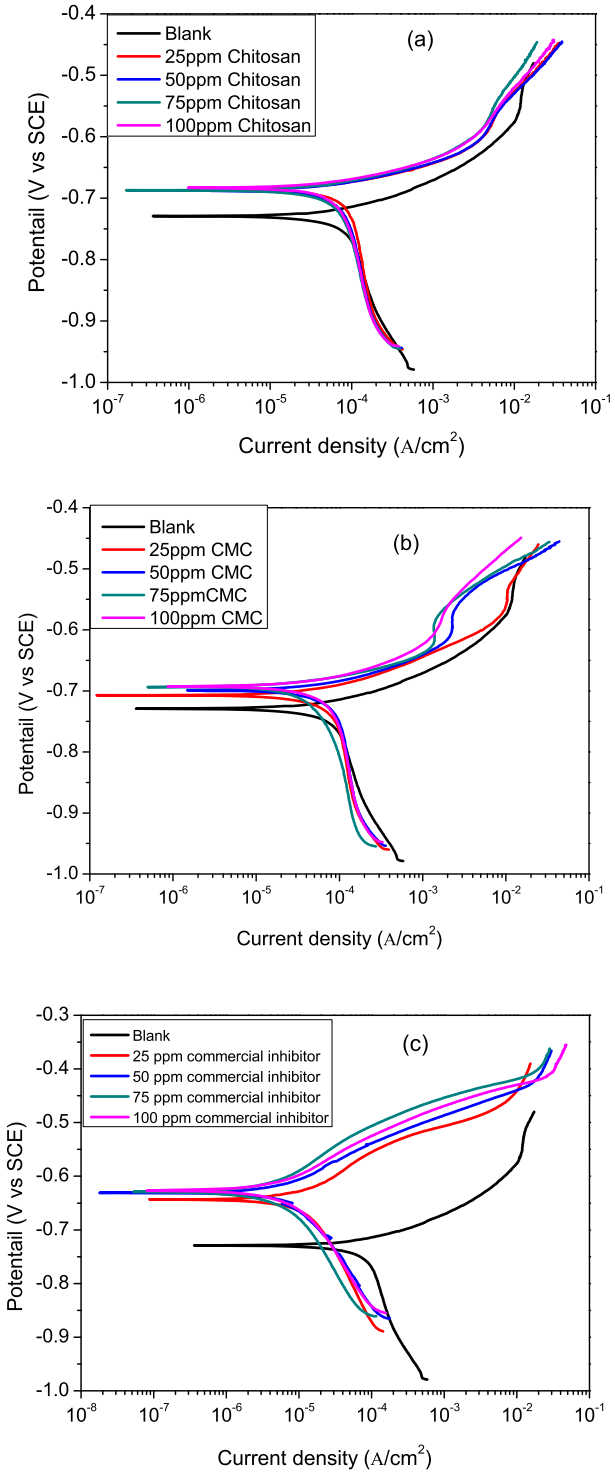

Fig. 4. Potentiodynamic polarization curves for API 5L X60 steel in CO_2-saturated 3.5% NaCl solution without and with varying concentrations of (a) Chitosan, (b) CMC and (c) commercial inhibitor at 25 °C.

where ρ is the surface area of the metal sample. Table 2 shows the values of corrosion current density (i_{corr}), corrosion potential (E_{corr}), and the anodic (β_a) Tafel slopes constants derived from the polarization curves. Compared to the blank solution, the values of i_{corr} decreased with the concentration of the three inhibitors; the commercial inhibitor had the least values (meaning it was the most protective) for API 5L X60 pipeline steel in CO_2-saturated saline solution followed by chitosan. The optimum concentration of the commercial inhibitor for steel protection

Table 2
Potentiodynamic polarization parameters for API 5L X60 steel corrosion in CO_2-saturated 3.5% NaCl solution without and with different concentrations of chitosan, CMC and commercial inhibitors at 25 °C.

Specimen	Concentration (ppm)	$-E_{corr}$ (mV/SCE)	i_{corr} (μA/cm^2)	β_a (mV/decade)	*IE* (%)
Blank	–	729	85.30	49	–
Chitosan	25	686	72.70	34	15
	50	687	63.70	36	25
	75	687	40.80	33	52
	100	683	38.20	25	55
CMC	25	707	64.70	46	24
	50	699	58.30	35	32
	75	693	43.80	36	49
	100	692	39.00	28	54
Commercial inhibitor	25	644	9.68	74	89
	50	631	8.38	86	90
	75	629	6.51	68	92
	100	627	5.62	82	93

in this medium seems to be 75 ppm, above which point the protective film breaks (also called "steady state concentration" [38]) and inhibition drops. This assertion is also reflected in the inhibition efficiency (*IE*%) values. Higher concentrations of chitosan have better inhibition performance; this could be attributed to the abundance of the amino-bearing glucosamine group in chitosan, which is capable of stable adsorption at the surface of API 5L X60 steel via its lone pairs of electrons. The current density values (37.2 and 39.8 μA/cm^2) were recorded for 100 and 75 ppm chitosan, respectively, against 37.9 and 41.0 μA/cm^2 for the same concentration range for CMC.

The values of *IE* for this technique were calculated in the absence and presence of inhibitors using the magnitudes of corrosion current density (Eq. (2)). The highest values of corrosion inhibition efficiency were recorded for 75 ppm commercial inhibitor (95%), 100 ppm chitosan (51%), and CMC (50%). The trend in *IE*% values follows that of i_{corr}, except that higher values are recorded for chitosan compared to CMC at 75 and 100 ppm; beyond this, *IE* values are comparable to commercial inhibitor. The values of E_{corr} do not change significantly in the presence of these inhibitors, conferring the status of a mixed-type inhibitor system with E_{corr} approaching nobler values; this is also reflected in the redox Tafel slopes, measured in mV/decade. Mixed-type inhibition systems are widely reported as possessing geometric blocking mechanisms on metal surfaces [38].

3.2. Effect of temperature

Besides the concentration of inhibiting species in the corrosive medium, corrosion inhibition process has been found to be dependent also on temperature. In this study, the effect of varying temperature was investigated in CO_2 saturated saline solution for API 5L X60 pipeline steel using EIS and PDP techniques in the presence of 100 ppm of each inhibitor conceived to give the highest inhibition efficiency in the previous test. Fig. 5 presents EIS spectra in the presence and absence of 100 ppm chitosan, CMC and commercial inhibitor at varying temperatures (25–60 °C) in (a–c) Nyquist, (d–f) Bode modulus and (g–i) phase angle formats. Inspection of the figure, revealed a one-time constant Nyquist curves with full capacitive loops with and without chitosan and CMC and two time constants for the commercial inhibitor. Generally, the shapes of the curves are maintained, indicating an unchanged corrosion mechanism at varying thermal conditions. For every inhibitor in this study, a reduced corrosion protection was revealed for API 5L X60 pipeline steel in the CO_2 saturated 3.5% NaCl solution as the temperature increased, evident in the decrease in the Nyquist semi-circle diameters.

Smaller semi-circle diameters representing higher corrosion rates for steel are revealed at 60 °C than the lower temperatures for all the inhibitors. The effect of temperature on corrosion inhibition is more

pronounced in the Bode plots (Fig. 5(d–f)), with a lowering of impedance (Z) of the interface at lower frequencies in the presence of the inhibitors compared to the blank solution. In the absence of the inhibitors, the API 5L X60 pipeline steel dissolved in the solution of the electrolyte at higher temperatures, as evident in the lowering of the impedance values, but this was observed to be reduced as the inhibitors were introduced into the corrosive medium.

Appropriate equivalent circuit models were used in fitting the impedance data and to provide an insight into the significance of temperature variation with corrosion inhibition. The derived electrochemical parameters from Nyquist plots for each inhibitor system after fitting the EIS data with these models in Fig. 3 between 25 and 60 °C are displayed in Table 3. From the Table 3, derived values of R_p decrease at the electrode/electrolyte interface as the temperature increases revealing increased corrosion rate for API 5L X60 pipeline steel in CO_2 saturated saline solution in the absence and presence of the corrosion inhibitors. Compared to chitosan, CMC shows slightly higher values of R_p with increase in temperature showing superior protection for API 5L X60 steel. The trend of charge transfer resistance values indicates that chitosan and CMC provided less protection compared to commercial inhibitor a hybrid composite of many anticorrosive additives at this temperature.

Generally, increase in corrosion rates of metals in the presence of inhibitors at higher temperatures can be attributed to desorption of the inhibitor molecules from the metal surface. This phenomenon is suggestive of physical adsorption being that molecules of the inhibitor displaced of adsorbed water molecules and attached to the metal surface without chemical bonding (via van der Waal forces) [30, 39]. However, high temperature favors the formation of layers of $FeCO_3$ on the electrode surface that further aids the protection of the substrate; this can be observed in the trend of *IE*. Adsorption of the molecules of the inhibitors tends to reduce the API 5L X60 steel corrosion at 25 °C; but at 40 °C, the *IE* values drops due to molecular desorption and then rises again, subsequently, at 60 °C. The percentage increase in the magnitude of *IE* between 40 and 60 °C for Chitosan, CMC, and commercial inhibitor were 89, 68 and 9%, respectively. The observed increment in the values

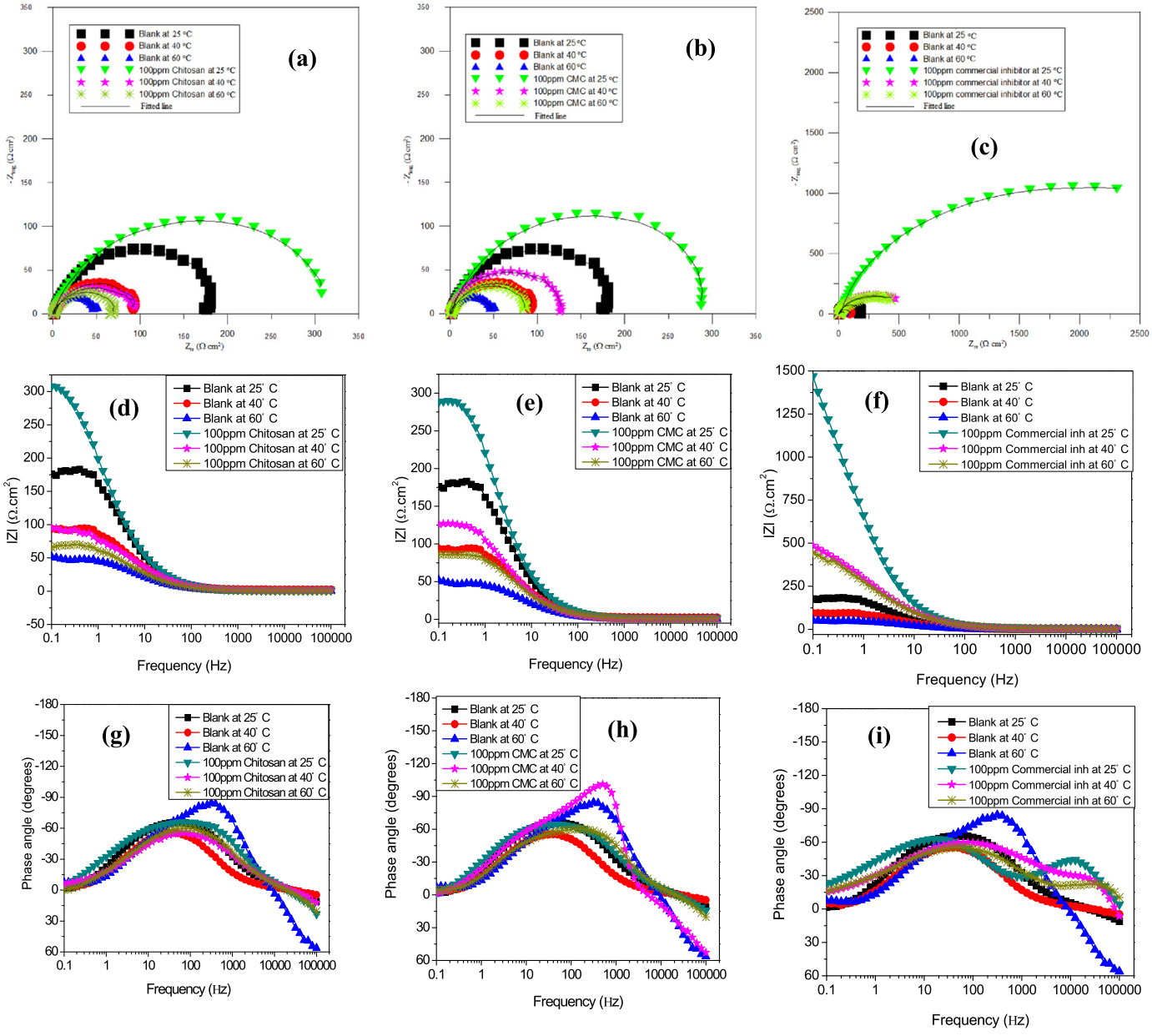

Fig. 5. Impedance plots for API 5L X60 steel in CO_2-saturated 3.5% NaCl solution in the absence and presence of 100 ppm of Chitosan, CMC and commercial inhibitor in (a) Nyquist, (b) Bode and (c) phase angle representations at different temperatures.

Table 3
EIS Parameters for API 5L X60 steel corrosion in CO_2-saturated 3.5% NaCl solution in the absence and presence of 100 ppm chitosan, CMC, and commercial inhibitor at different temperatures.

Specimen	Temperature (°C)	R_s (Ω cm^2)	CPE_f		R_f (Ω cm^2)	CPE_{dl}		R_{ct} (Ω cm^2)	$\chi^2 \times 10^{-3}$	R_p (Ω cm^2)	*IE* (%)
			Yo1 (μΩ s^n cm^{-2})	n_f		*Yo2* (μΩ s^n cm^{-2})	n_{dl}				
Blank	25	1.5	–	–	–	521	0.85	186.9	2.74	187	–
	40	2.7	–	–	–	818	0.81	94.8	0.87	95	–
	60	0.2	–	–	–	623	0.96	46.6	7.79	47	–
Chitosan	25	1.0	103	1.00	5.2	723	0.67	331.7	8.59	337	45
	40	1.5	98	0.99	1.6	1282	0.65	96.7	2.79	98	04
	60	0.9	164	1.00	2.4	1322	0.69	70.3	6.65	73	35
CMC	25	1.6	266	0.89	32.2	322	0.74	272.0	4.01	304	39
	40	0.2	439	1.00	3.9	3950	0.92	111.2	15.5	115	17
	60	0.9	178	0.98	8.5	1045	0.73	82.0	6.23	90	48
Commercial inhibitor	25	2.0	4	1.00	9.3	281	0.76	1601.0	2.76	1610	88
	40	0.9	455	0.67	10.6	33	0.92	434.1	4.97	445	79
	60	1.9	3	0.53	2.3	466	0.71	376.8	0.59	379	87

of the corrosion inhibition efficiency at 60 °C could be due to the formation of precipitate of corrosion products like $FeCO_3$ as well as Fe-inhibitor type complex which further protect the metal surface.

The effect of temperature was also studied for the corrosion of API 5L X60 pipeline steel in CO_2-saturated saline solution using the potentiodynamic polarization technique in the absence and presence of 100 ppm chitosan, CMC, and commercial inhibitor between 25 and 60 °C. The respective potentiodynamic polarization curves are shown in Fig. 6(a), (b) and (c) respectively, while the derived electrochemical parameters are listed in Table 4. The Tafel curves presented for the API 5L X60 pipeline steel in the solution of the test electrolyte (and within the thermal condition in this study) exhibit active dissolution without a distinctive transition to passivation within the potential range studied.

Since the values of i_{corr} can invariably give an idea of the corrosion rate for API 5L X60 pipeline steel in CO_2-saturated saline solution, the effect of temperature as it affects the corrosion rate of the substrate was evaluated from its magnitude. From the table, the values of i_{corr} were found to increase with temperature in the presence and absence of the corrosion inhibitors, with higher values recorded at 60 °C. The values of i_{corr} may be observed to gradually increase with temperature, with higher magnitudes recorded in the absence of the inhibitors at 60 °C. The shift in values of E_{corr} for the inhibitors relative to the blank seems more pronounced as the temperature rises, showing great influence of temperature variation on corrosion potential. From the results in Table 4, the minimum difference in these values is 46 mV for chitosan at 25 °C, confirming the mixed-type inhibitor earlier proposed. Some researchers [40, 41] have argued that differences in E_{corr} to a magnitude >85 mV for an inhibiting system relative to the blank solution implies a cathodic- or anodic-type system; otherwise, a mixed-type system is proposed. The increase in corrosion rate with increased temperature in the presence of the inhibitors in the CO_2-saturated saline electrolyte can be attributed to the desorption of the inhibitor molecules from the API 5L X60 pipeline steel surface at elevated temperatures. Since the formation of layers of $FeCO_3$ on the electrode surface is highly favored at higher temperatures, this surface phenomenon shifts the anodic and cathodic branches (mixed inhibitor systems) and further reduces the value of the corrosion current density. Reductions in the magnitude of current density are normally ascribed to the presence of more compact films on the surface of the electrode. Again, molecular adsorption inhibited the API 5L X60 steel dissolution at 25 °C; as the temperature increased to 40 °C, the *IE*% values dropped due to desorption of the adhered film. *IE*% values were found to increase again at 60 °C for the single- and multi-component inhibitor systems.

3.3. Effect of immersion time

In order to determine the effect of immersion time on the inhibitive action of the inhibitors for API 5L X60 pipeline steel in the CO_2-saturated saline solution, EIS measurements were performed between 1 and 24 h at 25 °C. Fig. 7 displays the changes in the electrochemical characteristics of the studied metal substrate in the considered corrosive medium with and without the addition of 100 ppm corrosion inhibitors (chitosan, CMC, and commercial inhibitor). From the similar nature of the Nyquist plots, we can determine that the mechanism of protection of the test metal did not change in the prolonged exposure period to the CO_2-saturated saline electrolyte. The gradual increase in the diameter of the Nyquist curve after 12 and 24-h exposure periods for chitosan indicates further protection of the steel substrate (Fig. 7(a–c)). Similar curves were recorded for CMC and commercial inhibitor between 1 and 24 h.

The calculated electrochemical impedance parameters derived after fitting with appropriate equivalent circuit models are shown in Table 5. The diameter of the Nyquist plots for commercial inhibitor is wider compared to chitosan and CMC. For this experiment, it is noted that CMC outperformed chitosan in showing better protection of the steel substrate upon prolonged immersion in the corrodent. This is evident in the improved R_p values at prolonged exposure times; 282 and 341 Ω cm^2 were recorded after 1 and 24-h exposure periods of API 5L X60 pipeline steel in the CO_2-saturated saline solution containing CMC. Similar exposure periods for chitosan recorded less R_p magnitude (175 and 254 Ω cm^2) for 100 ppm chitosan. The magnitude of API 5L X60 pipeline steel corrosion inhibition efficiency increased from 50% to 62% for CMC, which is greater than chitosan (19% to 34%), but much less than that obtained for commercial inhibitor (88% to 94%). The increased corrosion protection for the API 5L X60 pipeline steel surface in the presence of the inhibitors in the CO_2-saturated saline electrolyte can be attributed to the increased adsorption of the inhibitor molecules on the steel surface during prolonged exposure periods. The inhibition efficiency of the inhibitors is thus dependent upon the exposure periods of the API 5L X60 pipeline steel in the CO_2-saturated saline solution containing the inhibitors. The increased inhibition efficiency with longer exposure durations also reflects a strong molecular adsorption, and more protective film on the steel/electrolyte interface.

3.4. Surface analysis

Surface morphological examinations of the exposed steel specimens in uninhibited CO_2 saturated saline and inhibited solutions containing pure biopolymers as corrosion inhibitor compounds and commercial corrosion inhibitor were evaluated using SEM. Fig. 8 shows SEM images of the exposed API 5L X60 steel in CO_2 saturated saline solution in the (a) absence and presence of (b) 100 ppm Chitosan, (c) CMC compared with and (d) commercial corrosion inhibitor at room temperature after 24 h immersion. The steel substrate in the uninhibited blank solution shows severe corrosion on the surface with huge corrosion product mass due to uncontrolled dissolution as well as the other degradation episodes caused by the presence of carbonic acid in the solution of the electrolyte (Fig. 8a). While the steel substrate shows relatively uniform

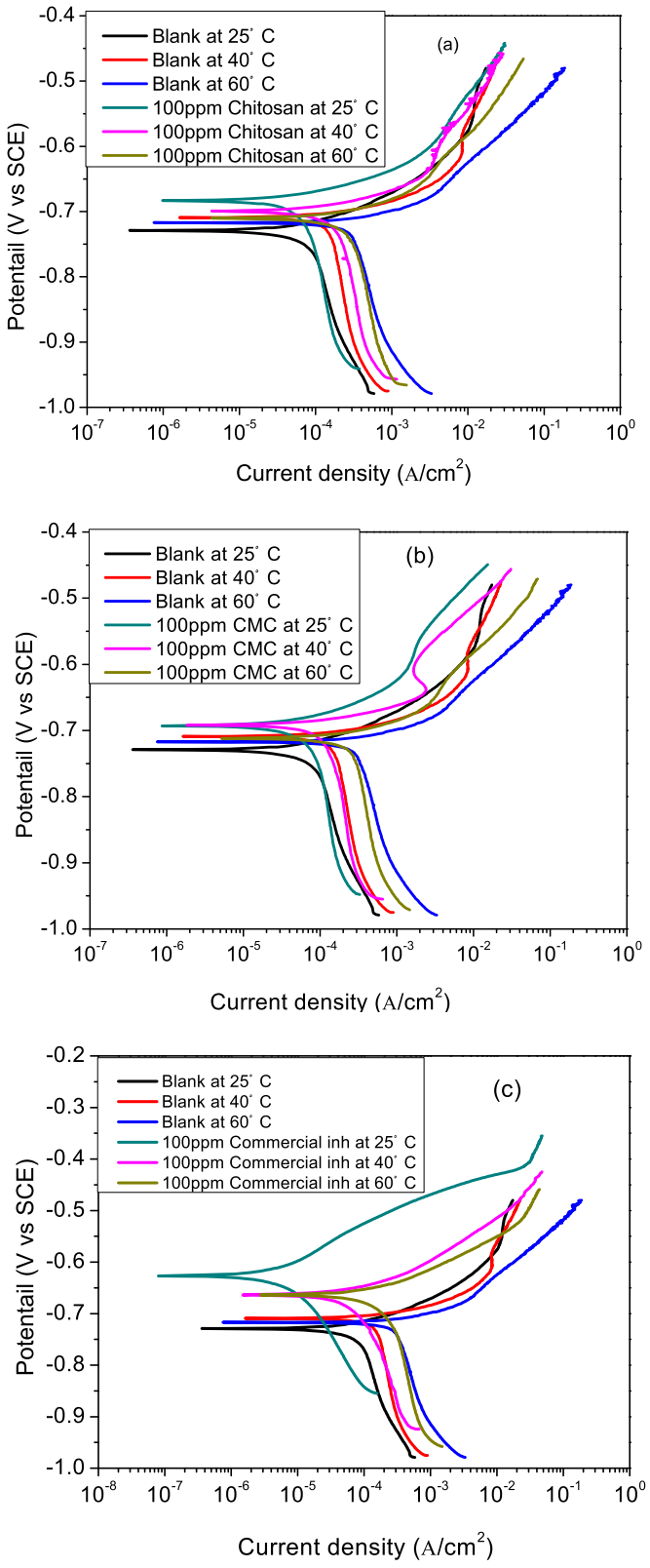

Fig. 6. Potentiodynamic polarization curves for API 5L X60 steel in CO_2-saturated 3.5% NaCl solution without and with 100 ppm of (a) Chitosan, (b) CMC and (c) commercial inhibitor at different temperatures.

corrosion in the presence of Chitosan, there seems to be evidence of localized attack for the coupon in 100 ppm CMC in the solution of the electrolyte. Generally, the presence of all the corrosion inhibitors shows visible reduction in corrosion of API 5L X60 pipeline steel to a great extent due to adsorption of molecules and subsequent formation of protective layers on the metal surface [28, 40]. Commercial inhibitor continues to show superior corrosion protection. This is evident in the clear SEM micrograph of the steel coupon in the solution of the electrolyte containing this inhibitor formulation — with few mold-like corrosion products and scales as continuous surface features.

Table 4
Potentiodynamic polarization parameters for API 5L X60 steel corrosion in CO_2-saturated 3.5% NaCl solution in the absence and presence of 100 ppm chitosan, CMC, and commercial inhibitor at different temperatures.

Specimen	Temperature (°C)	$-E_{corr}$ (mV/SCE)	i_{corr} (μA/cm²)	β_a (mV/dec.)	IE (%)
Blank	25	729	85.30	49	–
	40	709	120.00	25	–
	60	717	239.00	19	–
Chitosan	25	683	38.20	25	55
	40	699	113.00	29	06
	60	710	170.00	32	29
CMC	25	692	39.00	28	54
	40	692	95.80	24	20
	60	710	134.00	27	44
Commercial inhibitor	25	627	5.62	82	93
	40	664	30.10	29	75
	60	664	32.50	18	86

3.5. Adsorption isotherm

Corrosion inhibition is due to the direct adsorption of molecules of the inhibitors on the metal surface and/or could also involve the reaction of these compounds with a secondary compound to generate a film capable of forming a layer of protection at the metal/electrolyte interface. This surface adsorption process can be approximated by isotherm models using the magnitude of the surface coverage (θ; θ = IE/100) for a particular range of inhibitor concentration [42]. Selection of isotherm that best describe an adsorption process is often done by fitting θ values into different adsorption isotherm models and using the value of the linear regression parameter (R^2) as a gauge [22, 43]. This approach was adopted in this work and the best fit was found with Langmuir adsorption isotherm (R^2 value is in the range 0.92–0.99 (Table 6)). The Langmuir adsorption isotherm model has the form:

$$\frac{C}{\theta} = C + \frac{1}{K_{ads}} \tag{10}$$

where inhibitor concentration (C) is measured in ppm; inhibitor's surface coverage is denoted as θ and the K_{ads} is the equilibrium constant associated with interfacial molecular adsorption-desorption process. Fig. 9 shows the linear graphs obtained for the adsorption of chitosan, CMC, and the commercial inhibitor on the surface of the API 5L X60 pipeline steel substrate by plotting C/θ against C. The adsorption parameters derived from the Langmuir isotherm model are listed in Table 6. However, the gradients of curves are >1 required by an ideal Langmuir isotherm model. Non-unity slopes of Langmuir adsorption isotherm usually express inconsistency of experimental adsorption data with monolayer adsorption pattern proposed in the model. Langmuir adsorption isotherm also postulates uniequivalence inhibitor adsorption sites of surfaces as well as the independency in molecular adsorption with number of available sites [43, 44]. Since these conditions are not readily accessible in nature due to the heterogeneity of corrosion systems, adsorption can be addressed by redefining the Langmuir adsorption isotherm by introducing a dimensionless separation constant (K_L) (Eq. (11)): [45].

$$K_L = 1/(1 + K_{ads}C) \tag{11}$$

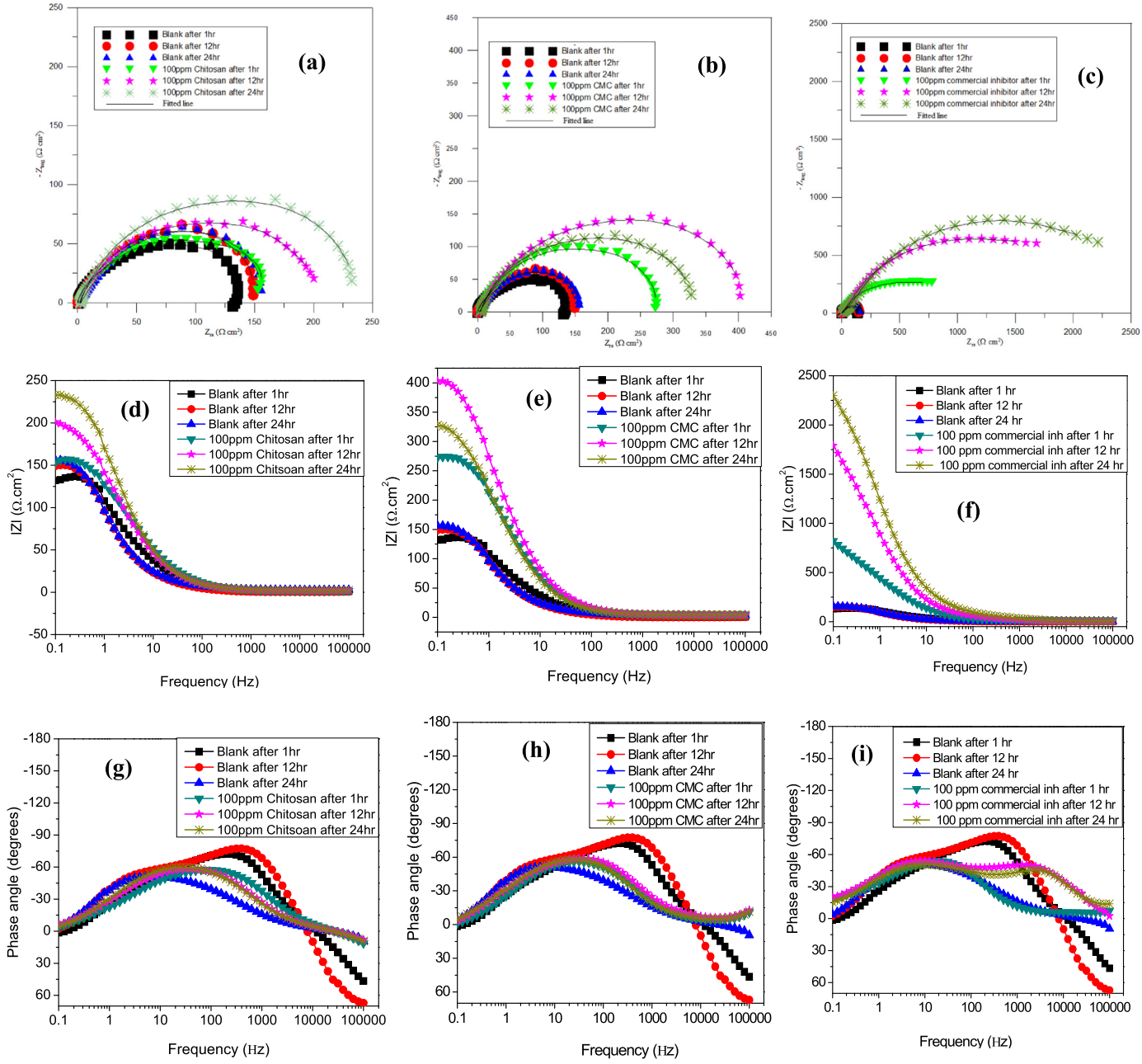

Fig. 7. Impedance plots for API 5L X60 steel in CO_2-saturated 3.5% NaCl solution in the absence and presence of 100 ppm of Chitosan, CMC and commercial inhibitor in (a) Nyquist, (b) Bode and (c) phase angle representations at different immersion times.

Table 5
EIS parameters for API 5L X60 steel corrosion in CO_2-saturated 3.5% NaCl solution in the absence and presence of 100 ppm chitosan, CMC, and commercial inhibitor at different immersion times.

Specimen	Time (h)	R_s (Ω cm^2)	CPE_f		R_f (Ω cm^2)	CPE_{dl}		R_{ct} (Ω cm^2)	$\chi^2 \times 10^{-3}$	R_p (Ω cm^2)	IE (%)
			$Yo1$ (μΩ s^n cm^{-2})	n_f		$Yo2$ (μΩ s^n cm^{-2})	n_{dl}				
Blank	1	–	–	–	–	1107	0.77	141.0	3.91	141	–
	12	–	–	–	–	1349	0.82	158.6	11.5	159	–
	24	–	–	–	–	694	0.85	168.4	2.08	168	–
Chitosan	1	1.8	70	0.69	2.9	969	0.63	172.3	2.18	175	19
	12	2.2	87	1.00	1.9	980	0.67	216.1	1.05	218	27
	24	2.4	82	1.00	2.4	754	0.71	251.8	1.45	254	34
CMC	1	4.6	474	0.79	217.8	505	1.00	64.6	1.72	282	50
	12	4.1	436	0.78	331.6	946	1.00	90.8	2.18	422	62
	24	4.3	573	0.78	289.9	2221	1.00	51.5	1.81	341	51
Commercial inhibitor	1	15.2	296	0.77	610.0	2472	0.68	552.3	2.66	1162	88
	12	3.1	40	0.82	48.2	209	0.67	2136.0	0.69	2184	93
	24	6.4	18	0.82	61.9	154	0.67	2681.0	0.54	2743	94

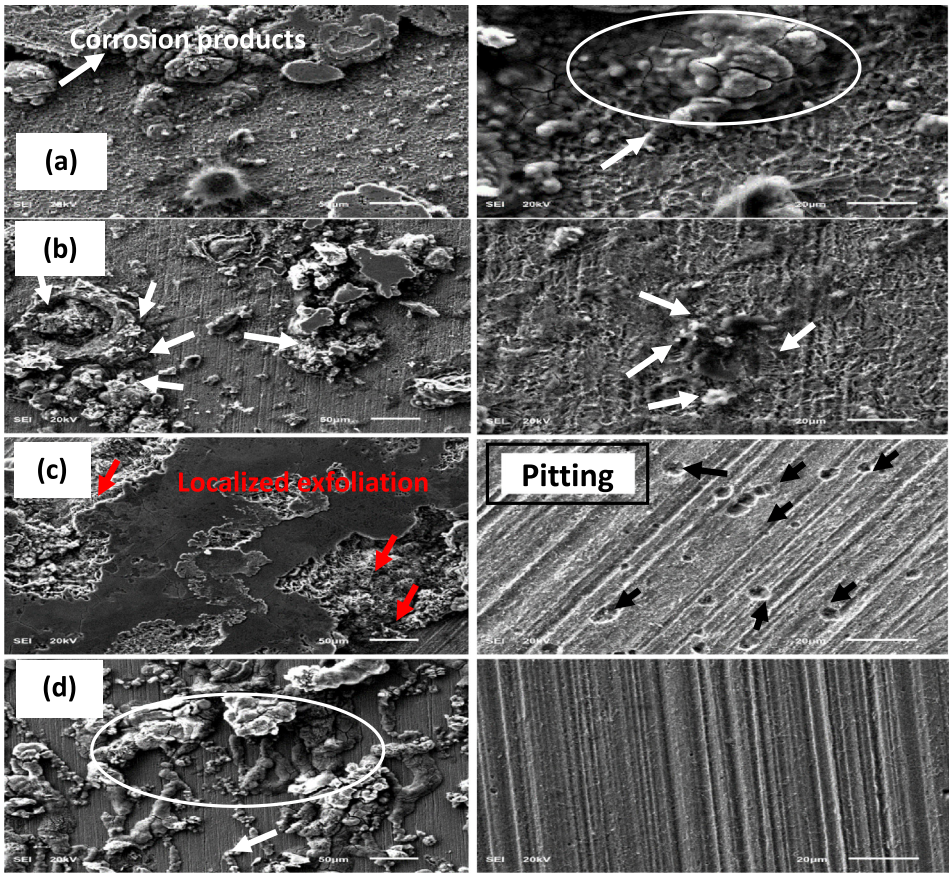

Fig. 8. SEM micrographs of corrosion products formed on API 5L X60 pipeline steel exposed to (a) blank (corrodent) CO_2 saturated 3.5% NaCl solution; and the corrodent containing (b) 100 ppm Chitosan; (c) 100 ppm CMC; (d) Commercial inhibitor at room temperature after 24 h immersion. [Right and left panels show 50 and 20 μm micrographs, respectively].

K_L = Separation factor of molecular adsorption

The calculated values of this dimensionless quantity are presented in Table 7 for the different inhibitor systems. The presented values of K_L for the single-component inhibitors and the commercial inhibitor are all less than unity ($K_L < 1$), thus showing favorable molecular adsorption and good fitting for the range of concentration of the inhibitors studied [45].

The magnitude of K_{ads} is empirically related to standard Gibbs free energy (ΔG_{ads}) of adsorption by Eq. (12):

$$\Delta G^{o}_{ads} = -RT\, In\left(1 \times 10^{6}\, K_{ads}\right) \quad (12)$$

where the absolute temperature, T is measured in K; the molar gas constant, R, is expressed in J/K/mol and the magnitude of the concentration of water molecules, 1×10^{-6}, is expressed in ppm or mg/L. The calculated values of K_{ads} (constant of adsorption–desorption process) are 0.0255, 0.0109 and 1.53, respectively, for chitosan, CMC and commercial inhibitor with −25.2, −23.0 and −35.3 kJ/mol being the designated magnitudes of ΔG_{ads} for the inhibitors (Table 6). The range of ΔG_{ads} are suggestive of electrostatic metal-inhibitor interaction for chitosan and CMC; that is, physisorption and mixed-mode of adsorption for commercial inhibitor, since its value is greater than −20 kJ/mol and less than −40 kJ/mol. Generally, ΔG^{o}_{ads} values up to −20 kJ/mol are consistent with a physical adsorption mechanism, while those lower than −40 kJ/mol define a chemical adsorption mechanism [46]. The negative magnitude of ΔG_{ads} is indicative of thermodynamic spontaneity associated with the adsorption process of the inhibitors onto the API 5L X60 pipeline steel surface.

Table 6
Langmuir adsorption parameters for API 5L X60 steel corrosion in the presence of the different inhibitor systems in CO_2-saturated 3.5% NaCl solution.

Inhibitor	ΔG^{o}_{ads} (kJ/mol)	K_{ads} ($g^{-1}L$)	Slope	R^2
Chitosan	−25.14	0.0255	2.29	0.97
CMC	−23.03	0.0109	1.45	0.92
Commercial inhibitor	−35.28	1.5300	1.11	0.99

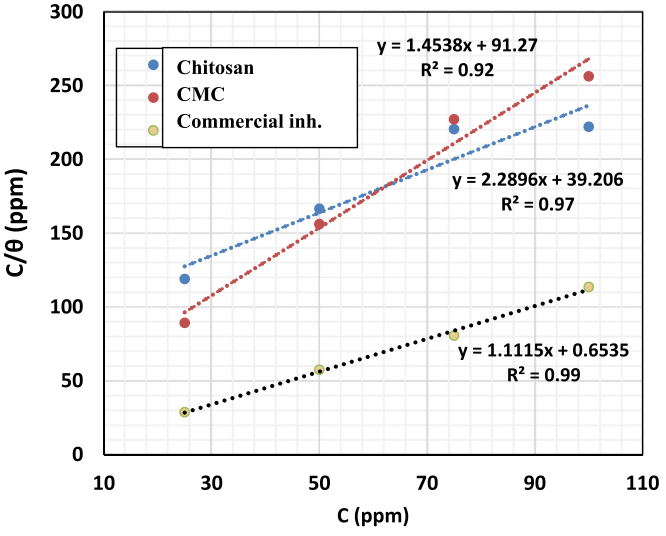

Fig. 9. Langmuir adsorption isotherm for the test inhibitors on API 5L X60 pipeline steel immersed in CO_2 saturated saline solution at 25 °C obtained from the EIS measurements.

Table 7
Values of dimensionless separation constant (K_L), derived from the Langmuir adsorption isotherm for chitosan, CMC, and Commercial inhibitor.

Concentration (ppm)	Chitosan	CMC	Commercial inhibitor
25	0.7850	0.6106	0.0254
50	0.6461	0.4395	0.0129
75	0.5489	0.3433	0.0086
100	0.4772	0.2817	0.0065

4. Conclusions

Two single component compounds, Chitosan and CMC, have been found to inhibit API 5L X60 pipeline steel corrosion in CO_2 saturated saline solution to some extent compared to commercial inhibitor, a typical multi-component inhibitor formulation used in the oil-field. The corrosion inhibition efficiency was found to be dependent on the concentration of the individual inhibitor; the temperature and the immersion period. Adsorption of molecules of the inhibitor on the surface of the API 5L X60 pipeline steel substrate has been approximated by Langmuir adsorption isotherm, and corrosion inhibition has been described in terms of assumptions of this model. The charge-transfer process and associated double-layer behavior of the metal/solution interface has been described to be related to the high-frequency capacitive loop of impedance spectra. SEM studies of the surface of the steel substrate in the solution of the electrolyte containing these inhibitors showed improved protection due to formation of anticorrosive films. API 5L X60 steel surfaces revealed more uniform and smoother surfaces. With a remarkable protection for steel in CO_2 saturated saline solution at a concentration as low as 100 ppm for chitosan and CMC, these single–component inhibitor compounds could under appropriate formulation in the presence of co-inhibitor(s) serve as anticorrosive additives for low carbon steel corrosion in CO_2-saturated NaCl environment as the commercial inhibitor with practical industrial applications.

Acknowledgements

The authors gratefully acknowledged King Fahd University for Petroleum and Minerals (KFUPM) and Centre of Research Excellence in Corrosion, KFUPM for providing the facilities to carry out the work.

References

[1] D.A. Lopez, W.H. Schreiner, S.R. de Sanchez, S.N. Simison, The influence of inhibitors molecular structure and steel microstructure on corrosion layers in CO_2 corrosion, Appl. Surf. Sci. 236 (2004) 77–97.
[2] C. Li, Effect of Corrosion Inhibitor on Water Wetting and Carbon Dioxide Corrosion In Oil-Water Two-Phase Flow, (PhD Thesis) Ohio University, 2009.
[3] M. Heydari, M. Javidi, Corrosion inhibition and adsorption behaviour of an amido-imidazoline derivative on API 5L X52 steel in CO_2-saturated solution and synergistic effect of iodide ions, Corros. Sci. 61 (2012) 148–155.
[4] D.M. Ortega-Toledo, J.G. Gonzalez-Rodriguez, M. Casales, L. Martinez, A. Martinez-Villafañe, CO_2 corrosion inhibition of X-120 pipeline steel by a modified imidazoline under flow conditions, Corros. Sci. 53 (2011) 3780–3787.
[5] M.W.S. Jawich, G.A. Oweimreen, S.A. Ali, Heptadecyl-tailed mono- and bis-imidazolines: a study of the newly synthesized compounds on the inhibition of mild steel corrosion in a carbon dioxide-saturated saline medium, Corros. Sci. 65 (2012) 104–112.
[6] J. Liu, W. Yu, J. Zhang, S. Hu, L. You, G. Qiao, Molecular modeling study on inhibition performance of imidazolines for mild steel in CO_2 corrosion, Appl. Surf. Sci. 256 (2010) 4729–4733.
[7] M.A.J. Mazumder, H.A. Al-Muallem, S.A. Ali, The effects of N-pendants and electron-rich amidine motifs in 2-(p-alkoxyphenyl)-2-imidazolines on mild steel corrosion in CO_2-saturated 0.5 M NaCl, Corros. Sci. 90 (2015) 54–68.
[8] A. Singh, K.R. Ansari, A. Kumar, W. Liu, C. Songsong, Y. Lin, Electrochemical, surface and quantum chemical studies of novel imidazole derivatives as corrosion inhibitors for J55 steel in sweet corrosive environment, J. Alloys Compd. 712 (2017) 121–133.
[9] H. Zhang, X. Pang, M. Zhou, C. Liu, L. Wei, K. Gao, The behavior of pre-corrosion effect on the performance of imidazoline-based inhibitor in 3 wt.% NaCl solution saturated with CO_2, Appl. Surf. Sci. 356 (2015) 63–72.
[10] X. Liu, P.C. Okafor, Y.G. Zheng, The inhibition of CO_2 corrosion of N80 mild steel in single liquid phase and liquid/particle two-phase flow by aminoethyl imidazoline derivatives, Corros. Sci. 51 (2009) 744–751.
[11] F.G. Liu, M. Du, J. Zhang, M. Qiu, Electrochemical behavior of Q235 steel in saltwater saturated with carbon dioxide based on new imidazoline derivative inhibitor, Corros. Sci. 51 (2009) 102–109.
[12] D.M. Ortega-Toledo, J.G. Gonzalez-Rodriguez, M. Casales, M.A. Neri-Florez, A. Martinez-Villafañe, The CO_2 corrosion inhibition of a high strength pipeline steel by hydroxyethyl imidazoline, Mater. Chem. Phys. 122 (2010) 485–490.
[13] P.C. Okafor, X. Liu, Y.G. Zheng, Corrosion inhibition of mild steel by ethylamino imidazoline derivative in CO_2-saturated solution, Corros. Sci. 51 (2009) 761–768.
[14] G. Zhang, C. Chen, M. Lu, C. Chai, Y. Wu, Evaluation of inhibition efficiency of an imidazoline derivative in CO_2-containing aqueous solution, Mater. Chem. Phys. 105 (2007) 331–340.
[15] D.A. Lopez, S.N. Simison, S.R. de Sanchez, Inhibitors performance in CO_2 corrosion: EIS studies on the interaction between their molecular structure and steel microstructure, Corros. Sci. 47 (2005) 735–755.
[16] V.M. Abbasov, S.R. Gadjiyeva, R.S. Magerramov, N.S. Akhmedov, S.R. Rasulov, Influence of potassium salts of nitro derivative high α-olefins in 1% NaCl solution saturated with CO_2 on steel corrosion, Azerbaijani Oil Ind. 8 (2010) 1–4.
[17] W.J. Benton and L.P. Koskan, Inhibition of carbon dioxide corrosion of metals, US Patent 5607623 A, 1997.
[18] J. Killaars, P. Finley, SPE International Symposium on Oilfield Chemistry. Houston, Texas, SPE 65044, 2001.
[19] I. Arukalam, I. Madufor, O. Ogbobe, E.E. Oguzie, Inhibition of mild steel corrosion in sulphuric acid medium by hydroxyethyl cellulose, Chem. Eng. Comm. 202 (2014) 112–122.
[20] E. Bayol, A.A. Gürten, M. Dursun, K. Kayakirilmaz, Adsorption behavior and inhibition corrosion effect of sodium carboxymethyl cellulose on mild steel in acidic medium, Wuli Huaxue Xuebao/Acta Phys. Chim. Sin. 24 (2008) 2236–2242.
[21] H. Bentrah, Y. Rahali, A. Chala, Gum Arabic as an eco-friendly inhibitor for API 5L X42 pipeline steel in HCl medium, Corros. Sci. 82 (2014) 426–431.
[22] M.M. Solomon, S.A. Umoren, I.I. Udosoro, A.P. Udoh, Inhibitive and adsorption behaviour of carboxymethyl cellulose on mild steel corrosion in sulphuric acid solution, Corros. Sci. 52 (2010) 1317–1325.
[23] S.A. Umoren, M.J. Banera, T. Alonso-Garcia, C.A. Gervasi, M.V. Mirífico, Inhibition of õmild steel corrosion in HCl solution using chitosan, Cellulose 20 (2013) 2529–2545.
[24] S.A. Umoren, I.B. Obot, A. Madhankumar, Z.M. Gasem, Performance evaluation of pectin as ecofriendly corrosion inhibitor for X60 pipeline steel in acid medium: experimental and theoretical approaches, Carbohy. Polym. 124 (2015) 280–291.
[25] R. Geethanjali, A. Ali, F. Sabirneeza, S. Subhashini, Water-soluble and biodegradable pectin-grafted polyacrylamide and pectin-grafted polyacrylicacid: electrochemical investigation of corrosion-inhibition behaviour on mild steel in 3.5% NaCl media, Ind. J. Mater. Sci. (2014)https://doi.org/10.1155/2014/356075.
[26] B.J. Usman, S.A. Umoren, Z.M. Gasem, Inhibition of API 5L X60 steel corrosion in CO_2 –saturated 3.5% NaCl solution by tannic acid and synergistic effect of KI additive, J. Mol. Liq. 237 (2017) 146–156.
[27] P.M. Gil, J. Manuel, R. Domínguez, I. Mexicano, R. Lindsay, Corrosion inhibition performance of 2-mercaptobenzimidazole in sweet oilfield conditions, NACE Corrosion 2014, pp. 1–9 , Paper No. 4109.
[28] S.A. Umoren, Z.M. Gasem, I.B. Obot, Natural products for material protection: inhibition of mild steel corrosion by date palm seed extracts in acidic media, Ind. Eng. Chem. Res. 52 (2013) 14855–14865.
[29] S.A. Umoren, Z.M. Gasem, I.B. Obot, Date palm (*Phoenix dactylifera*) leaf extract as eco-friendly corrosion inhibitor for mild steel in 1 M hydrochloric acid solution, Anti-Corros. Method Mater. 62 (2015) 19–28.
[30] S.A. Umoren, Y. Li, F.H. Wang, Synergistic effect of iodide ion and polyacrylic acid on corrosion inhibition of iron in H_2SO_4 investigated by electrochemical techniques, Corros. Sci. 52 (2010) 2422–2429.
[31] S.A. Umoren, Polypropylene glycol: A novel corrosion inhibitor for X60 pipeline steel in 15% HCl solution, J. Mol. Liq. 219 (2016) 946–958.
[32] C. Jeyaprabha, S. Sathiyanarayanan, G. Venkatachari, Influence of halide ions on the adsorption of diphenylamine on iron in 0.5 M H_2SO_4 solutions, Electrochim. Acta 51 (2006) 4080–4088.
[33] S. Kirtay, Preparation of hybrid silica sol-gel coatings on mild steel surfaces and evaluation of their corrosion resistance, Prog. Org. Coat. 77 (2014) 1861–1866.
[34] T. Pojtanabuntoeng, M. Salasi, An electrochemical study of carbon steel CO_2 corrosion in the presence of monoethylene glycol: the effects of pH and hydrodynamic conditions, Electrochim. Acta 258 (2017) 442–452.
[35] G. Ruhi, O.P. Modi, A.S.K. Sinha, I.B. Singh, Effect of sintering temperatures on corrosion and wear properties of sol–gel alumina coatings on surface pre-treated mild steel, Corros. Sci. 50 (2008) 639–649.
[36] C. De Waard, D.E. Milliams, Carbonic acid corrosion of steel, Corrosion 31 (1975) 177–181.
[37] J. Tkacz, J. Minda, S. Fintová, J. Wasserbauer, Comparison of electrochemical methods for the evaluation of cast AZ91 magnesium alloy, Materials 9 (2016) 925.
[38] R. Lopes-Sesenes, G.F. Dominguez-Patiño, J.G. Gonzalez-Rodriguez, J. Uruchurtu-Chavarin, Effect of flowing conditions on the corrosion inhibition of carbon steel by extract of *Buddleia perfoliata*, Int. J. Electrochem. Sci. 8 (2013) 477–489.
[39] S.A. Umoren, O. Ogbobe, I.O. Igwe, E.E. Ebenso, Inhibition of mild steel corrosion in acidic medium using synthetic and naturally occurring polymers and synergistic halide additives, Corros. Sci. 50 (2008) 1998–2006.
[40] P.C. Okafor, Y. Zheng, Synergistic inhibition behaviour of methylbenzyl quaternary imidazoline derivative and iodide ions on mild steel in H_2SO_4 solutions, Corros. Sci. 51 (2009) 850–859.
[41] S.S. Abd El Rehim, H.H. Hassan, M.A. Amin, Corrosion inhibition of aluminum by 1,1 (lauryl amido)propyl ammonium chloride in HCl solution, Mater. Chem. Phys. 70 (2001) 64–72.

[42] K. Bouhrira, A. Chetouani, D. Zerouali, B. Hammouti, A. Yahyi, A. Et-Touhami, R. Yahyaoui, R. Touzan, Theoretical investigation of inhibition of the corrosion of A106 steel in NaCl solution by di-n-butyl bis(thiophene-2-carboxylato-O,O0)tin (IV), Res. Chem. Intermed. 40 (2014) 569–586.
[43] E.E. Oguzie, C.K. Enenebeaku, C.O. Akalezi, S.C. Okoro, A.A. Ayuk, E.N. Ejike, Adsorption and corrosion-inhibiting effect of *Dacryodis edulis* extract on low-carbon-steel corrosion in acidic media, J. Coll. Interf. Sci. 349 (2010) 283–292.
[44] K.F. Khaled, A. El-Maghraby, Experimental, Monte Carlo and molecular dynamics simulations to investigate corrosion inhibition of mild steel in hydrochloric acid solutions, Arab. J. Chem. 7 (2014) 319–326.
[45] E.A. Noor, Evaluation of inhibitive action of some quaternary N-heterocyclic compounds on the corrosion of Al–Cu alloy in hydrochloric acid, Mater. Chem. Phys. 114 (2009) 533–541.
[46] S. Bilgic, M. Sahin, The corrosion inhibition of austenitic chromium-nickel steel in H_2SO_4 by 2-butyn-1-ol, Mater. Chem. Phys. 70 (2001) 290–295.